CLASSIFICATION OF VEGETATION COMMUNITIES IN THE TROPICAL SAVANNAS OF NORTHERN AUSTRALIA USING AIRSAR DATA

Authors: Carl H. Menges[1], Jakob J. van Zyl[2], Waqar Ahmad[1], and Greg J. E. Hill[1]

[1] Faculty of Science, Northern Territory University, Darwin NT 0909, Australia
[2] Jet Propulsion Laboratory, California Institute of Technology, 4800 Oak Grove Drive Pasadena, CA 91109, USA

ABSTRACT: Radar remote sensing offers great potential for resource management in tropical regions. This paper outlines a processing methodology for AirSAR data for land cover classification using standard image processing software. The side looking nature of the instrument introduces significant variation in incidence angle from an airborne platform. The changes introduced by variation in incidence angle are dependent on the land cover and can, therefore, not be removed by mathematical modeling unless the exact ground cover composition is known. The proposed methods for the removal of this effect are based on the statistical comparison of lines of data with constant incidence angle. It is shown, for the vegetation communities in a coastal tropical savanna landscape in Australia's Northern Territory, that a successful correction method for the effects of incidence angle variation can be implemented. The elimination of backscatter dependence on incidence angle allows the qualitative discrimination of land cover types using a supervised technique. A maximum likelihood classification of the data achieved an overall accuracy of 87.2% for six land cover types. The separation of classes is based on structural rather than species differences. Subdivision of the *Eucalypt* forest class derived from the supervised approach delineates distinct classes but further research is required to determine the biophysical parameters of vegetation determining the resulting stratification.

1. INTRODUCTION

Digital image classification is an important tool for resource management. Remote sensing data have been used widely by ecologists to delineate structural and compostional boundaries of vegetation communities and map the distribution of these communities throughout the landscape. The use of Synthetic Aperture Radar (SAR) for mapping resources and monitoring temporal changes in ecosystems is desirable because SAR is able to penetrate cloud cover, thus allowing resource monitoring in all regions of the globe and at all times of the year. Furthermore, it is highly likely that the analysis of SAR data will provide additional information about ecosystems, as data collected from a different part of the electromagnetic spectrum is determined by different characteristics of the surface and vegetation cover. Radar imagery, for example, has

been shown to allow separation of forest classes which appear identical using optical data by detecting flooding beneath a closed canopy (Hess et al. 1995).

Much research using SAR data has focused on the theoretical development of backscatter models for a range of forest types (Dong et al. 1995, Borgeaud 1994, Chuah and Kung 1994, Whitt and Ulaby 1994, McDonald and Ulaby 1993, Wang et al. 1993a, b, c, Chauhan et al. 1991, Sun et al. 1991, Durden et al. 1989, Sun and Simonett 1991). These models aid the understanding of the relative importance of surface characteristics in determining backscatter. Inversion of such complex models, however, for retrieval of surface characteristics from radar data is virtually impossible (Kasischke et al. 1997).

Maximum likelihood approaches have been used with high land cover discrimination accuracy for given study areas (Ranson and Sun 1997, Saatchi et al. 1997, deGrandi et al. 1994, Lemoine et al. 1994, Ranson and Sun 1994 , Rignot et al. 1994b). Decision trees (Hess et al. 1995), fuzzy classifiers (Du and Lee 1996) and image segmentation (Rignot and Chellappa 1992, Dong et al. 1998) have also been used for image analysis.

This study presents a means of reducing the effect of incidence angle variation within the AirSAR data based on the statistical comparison of the data values. The procedure is based on the premise that all 'range lines', lines parallel to the flight line with constant incidence angle, contain a similar range of land cover. That is, the land cover composition of the study area does not vary significantly in range direction. The correction of the data for incidence angle effects allows the qualitative comparison of data values using a standard image classification methodology.

2. STUDY AREA

The savannas of northern Australia occupy approximately 25% of the Australian continental landmass. Climate is monsoonal with more than 95% of the annual rainfall (average 1700 mm) falling in the summer months of October to April. While an annual monsoon is predictable the timing and onset of the monsoons varies between years (Taylor and Tulloch 1985). Maximum daily temperatures and evaporation rates remain high throughout the year, ranging from 35 ^{o}C in the wet season to 31 ^{o}C during the dry season (Hickey, 1985) and evaporation rates of about 6-8 mm per day (Hutley *et al*. 1999). Distinct rainfall, temperature and humidity variation within these periods have created a diverse assemblage of savanna vegetation in northern Australia. This varies from well vegetated areas to sparsely vegetated areas and the composition and structure appears to be governed to a large extent by soil water availability and to a lesser extent nutrient availability (Willams *et al.* 1996), with fire also being an important determinant of savanna structure (Andersen *et al.* 1998).

The current study was conducted in the Gunn Point region approximately 50 km east of Darwin (130^{0} 45$^{'}$E, 12^{0} 30$^{'}$ S) in the Northern Territory (Figure 1). The area was dominated by *E. miniata/E. tetrodonta* open forests, a dominant forest type north of the 1200mm isohyet. The area was chosen due to the availability of recently acquired digital and other ancillary data such as ground survey data, vegetation type and land system/units maps. The *E. miniata/E. tetrodonta* open forests form the matrix within which other important vegetation communities occur, ranging from

wetlands to closed monsoon forests. Soils in the area are characterised by red and yellow sandy clay loams derived from highly weathered laterites of the Koolpinyah plateau (Bowman and Wrightman 1986). The topography of the study area is flat with no significant variation in elevation.

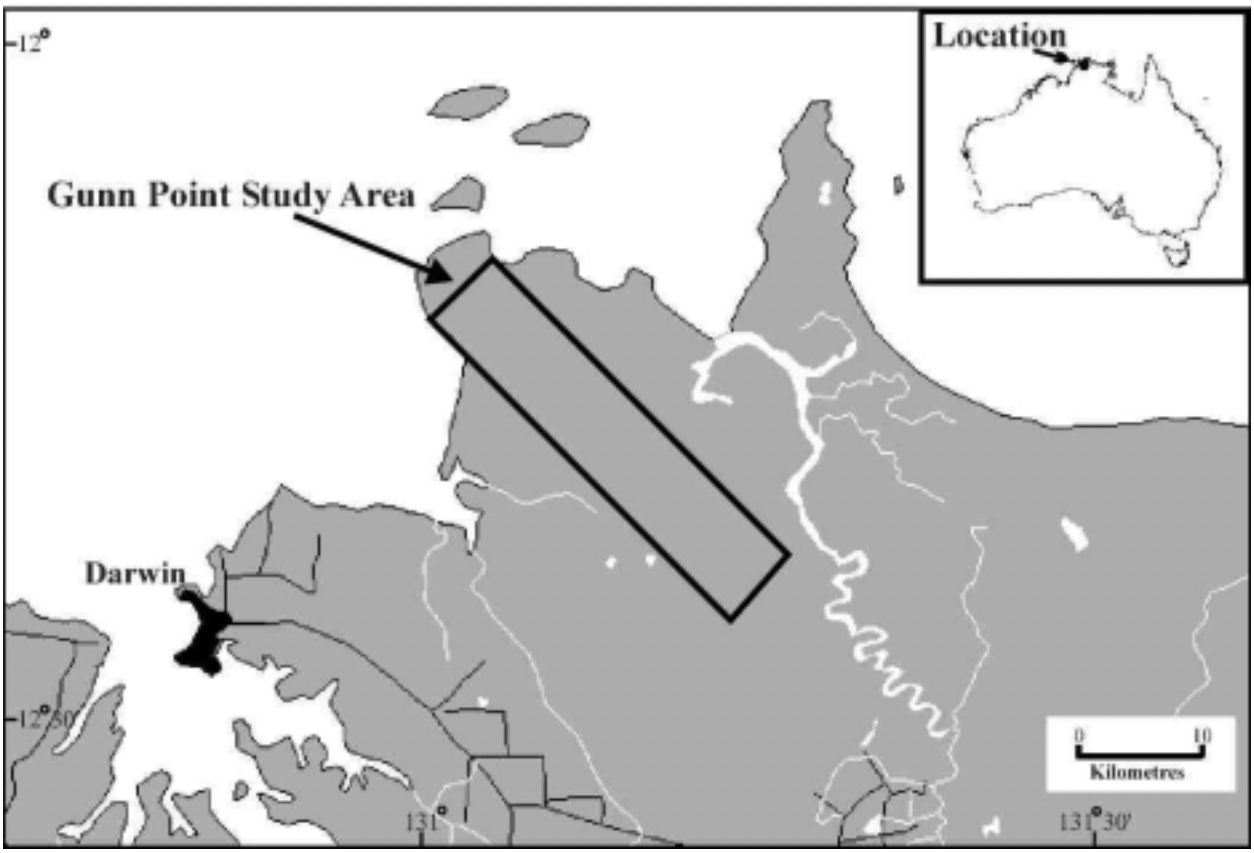

Figure 1. *Location of the Study Area*

3. DATA AND METHODOLOGY

The JPL (Jet Propulsion Laboratory) AIRSAR system was flown over the study site on board a DC-8 on the 23rd of November 1996. The AIRSAR acquired backscatter data at C-band (wavelength=5.6 cm, frequency=5.3 Ghz), L-band (23.9 cm, 1.25 Ghz) and P-band (67.0 cm, 0.44 Ghz) in four transmit / receive polarizations (HH, VV, HV, VH). Local time of data acquisition was 11.00 am under dry weather conditions with some cloud present. The AIRSAR data were processed as a 60km strip product by JPL's Radar Data Center using version 6.1 of the integrated processor, and supplied in 18 look compressed Stokes matrix format. The look angle ranges from 22.6 degrees to 61.7 degrees in the range direction.

The Stokes Matrix for polarimetric SAR data is a 4x4 matrix (van Zyl and Ulaby, 1990). Due to the assumption of symmetry (i.e. $S_{hv} = S_{vh}$) and averaging as part of the multi-look

processing a maximum of nine independent numbers need to be stored for each image pixel (Zebker and van Zyl, 1991). The compressed Stokes Matrix as processed by JPL's Radar Data Centre, therefore, contains 10 bytes of information per pixel, with two bytes being used to store the total power.

Nine independent elements describing the scattering behaviour can be extracted for each of the three frequency bands (see table 1). Five of these components that contain valuable information (Baker et al. 1994) are considered here. The three bands containing the magnitude of the backscatter at HH, VV and HV polarization as well as the real and imaginary component of the co-polarized backscatter. The latter two components can be used to compute the HH-VV phase difference and the correlation coefficient. The raw AirSAR data is shown as a colour composite in figure 2 for the three available frequency bands.

Table 1. The Nine Independent Scattering Elements Contained in the Compressed Stokes Matrix

Sacttering element	**Description**
$<S_{HH}S_{HH}^{*}>$	Magnitude of HH return
$<S_{VV}S_{VV}^{*}>$	Magnitude of VV return
$<S_{HV}S_{HV}^{*}>$	Magnitude of HV return
$Re<S_{HH}S_{VV}^{*}>$	Real part of HH-VV co-polarised return
$Im<S_{HH}S_{VV}^{*}>$	Imaginary part of HH-VV co-polarised return
$Re<S_{HH}S_{HV}^{*}>$	Real part of HH-HV cross-polarised return
$Im<S_{HH}S_{HV}^{*}>$	Imaginary part of HH-HV cross-polarised return
$Re<S_{HV}S_{VV}^{*}>$	Real part of HV-VV cross-polarised return
$Im<S_{HV}S_{VV}^{*}>$	Imaginary part of HV-VV cross-polarised return

The co-polarised returns were corrected for incidence angle using the LUT method. This method, is based on the correction technique outlined in Menges et al. (1999a, 1998). Here, the range line at the nominal incidence angle, is used as a look up table to match values of other rangelines. The AIRSAR data are used as well as the numerically sorted frequency distribution data of the rangelines generated in the previous stage. The procedure operates on a pixel by pixel basis on the AIRSAR data. The backscatter value of each pixel is noted together with its range distance. This backscatter value is searched for in the frequency distribution look up table at the same range line. In the numerically sorted frequency distribution look up table the row number at which the value is found indicates the percentile value of the cumulative frequency of the value's occurrence for that particular range line. Now the value associated with this cumulative frequency in the norm line can be determined and written to the "corrected" image.

The magnitude components of the SAR data set were corrected for the effect of variation in incidence angle using the slope of the linear regression determined for each line of constant incidence angle versus the norm line (Menges et al. 1999b). The values within the lines are numerically sorted for this purpose and the slope of the regression applied to the individual lines of data.

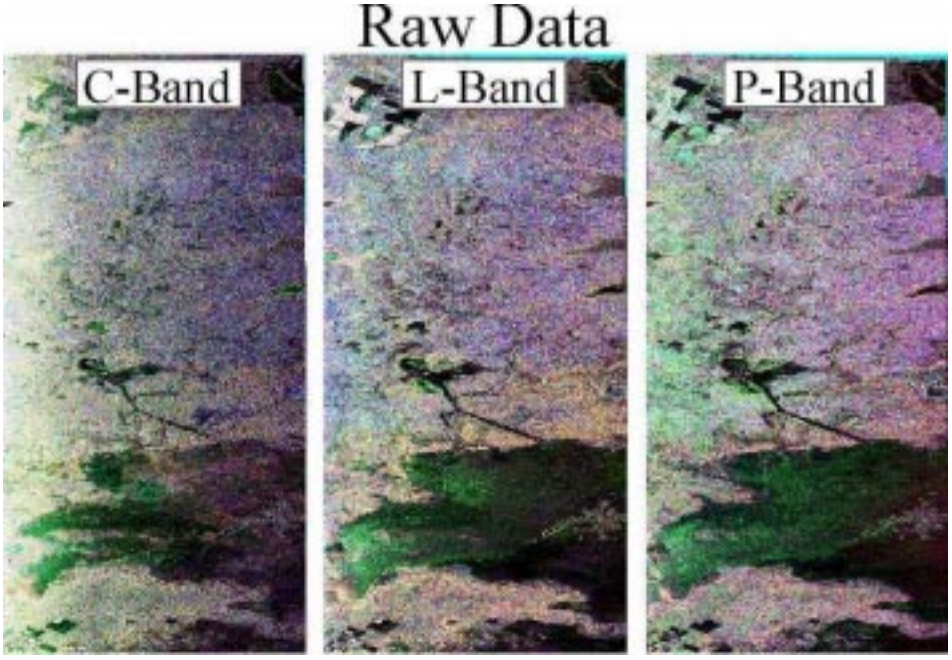

Figure 2. *Colour composites of the raw AirSAR data showing the HV, VV, and HH polarizations as RGB for the C-,L- and P-Band.*

As classification procedures such as the Maximum Likelihood classifier are based on the assumption of normal distribution within training samples, the magnitude channels were transformed to a logarithmic scale, that is decibel values. A mean 3 x3 filter was applied to all channels before this logarithmic transformation to reduce the effective resolution of the data approximating the optimal resolution for the detection of these ecological units (Menges et al. 1999c) and to reduce the speckle. The data is supplied by JPL as an 18-look average. Calculation of the Equivalent Number of Looks (ENL) as the ratio of the square of the mean divided by the variance for a homogeneous distributed target resulted in a value of 6.3 for the raw data. The ENL for the mean filtered intensity data equals 26.4 using the same target.

From the total of 15 channels available for the classification, 11 were chosen as input to the classification. This selection was based on the evaluation of separability between training area signatures using the transformed divergence measure (Menges et al. 1999d).

4. RESULTS

The colour composites of the raw data (figure 2) clearly show the ‘incidence angle contamination’. This is most prominent at the C-Band. The comparison of the frequency distribution along range lines as shown in the density sliced imaged (figure 3) offers a means of assessing the effect of incidence angle in a study area and a means for correcting the effect without requiring detailed knowledge of the land cover composition. For clarity, the numerically sorted data of all the available channels shown in figure 3 have been density sliced at one dB intervals. The data value for one of the intervals is shown in the figure to provide an indication of the range of values present in the data for the study area at the different bands and polarisations. It can be seen that in the medium range of backscatter values, the linear relationship to incidence

angle is confirmed. This clearly does not hold for higher and lower backscatter intensities, where the relationship appears non-linear.

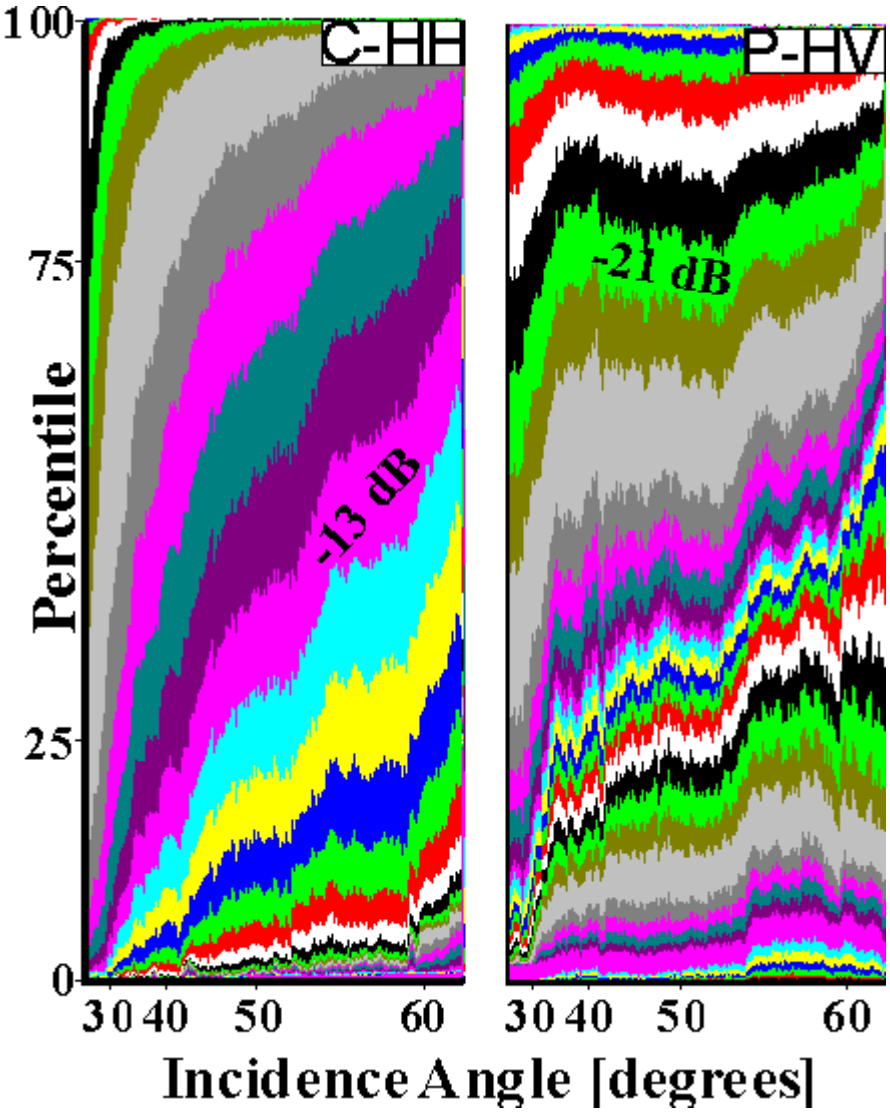

Figure 3. *Frequency distribution images of the numerically sorted data for C-HH and P-HV. A density slice was applied for clarity at 1 dB intervals*

A comparison of the norm line values with arbitrarily chosen rangelines in the near and far range was used to determine the validity of applying a linear regression to the data sets. The numerically sorted data in the lines to be regressed was found to have very high correlation coefficients (see Table 2). For the near range lines tested, at an incidence angle of 33 degrees, the correlation coefficients exceeded 0.99 for all scattering components. The lowest value for the far range lines tested, at an incidence angle of 60 degrees, was 0.92 for the real part of the HH VV co-polarized return in L-Band. A graphical representation of some of the relationships between the two rangelines tested and the norm line is shown as a crossplot in figure 4. Three examples have been chosen for backscatter magnitude components and one for the components of the HH VV co-polarized return. The examples chosen are typical of the relationships observed. For the rangeline data with an incidence angle of 60 degrees the relationships show non-linear behaviour

at very low data values. The extent of this curvature varies between scattering elements and frequency bands but is present throughout.

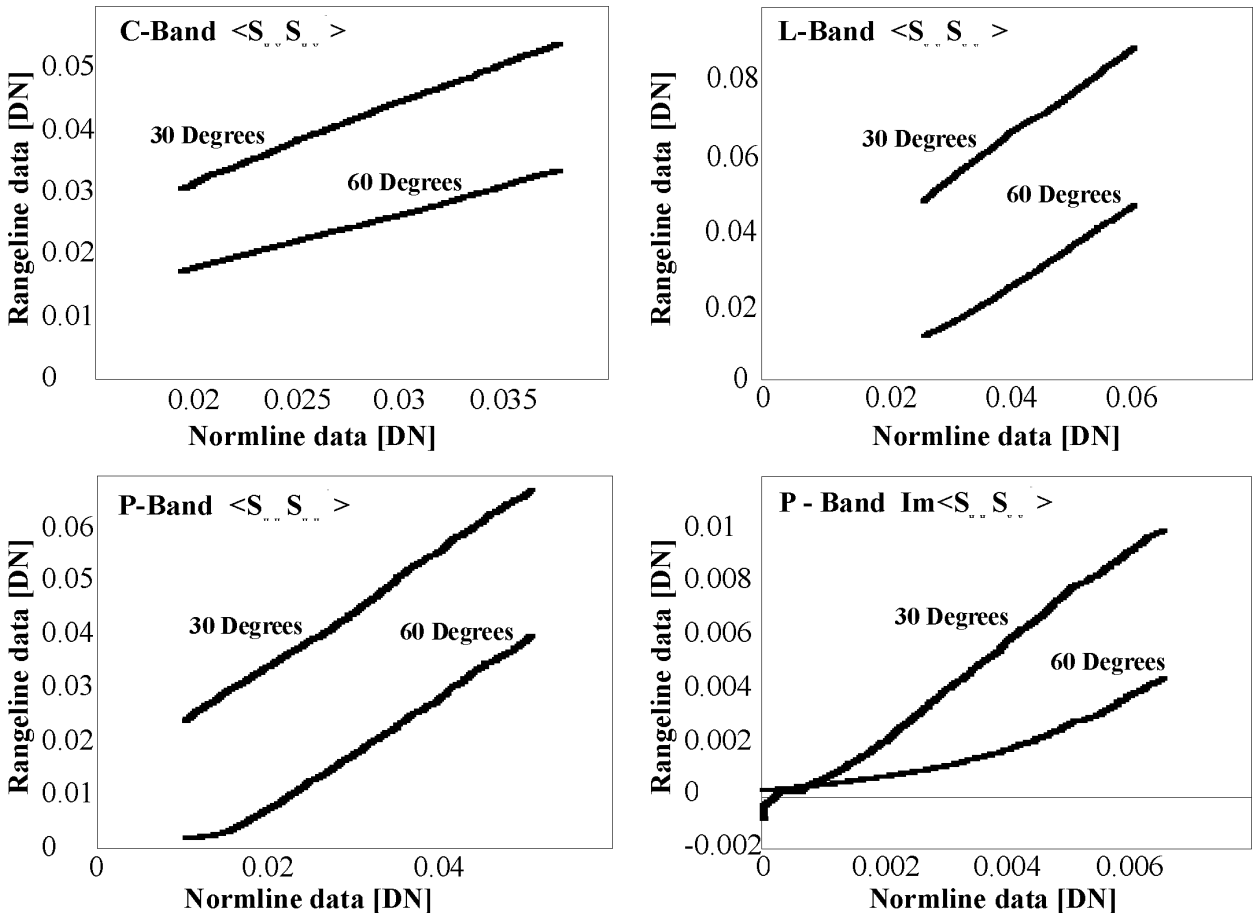

Figure 4. *Numerically sorted SAR data from 30 and 60 degrees incidence angle graphed against the values from the norm line at 48 degrees.*

Table 2. Correlation Coefficients for the Linear Regression of two Lines in the Near (33 degrees incidence angle) and Far Range (60 degrees incidence angle) Versus the Norm Line. The Values Obtained at All Three Frequency Bands Available for the Five Scattering Elements are Shown.

Near Range Line vs Norm Line				Line 2300 vs Norm Line			
BAND	C	L	P	BAND	C	L	P
$<S_{HH}S_{HH}^{*}>$	0.9988	0.9942	0.9943	$<S_{HH}S_{HH}^{*}>$	0.9971	0.9891	0.9899
$<S_{VV}S_{VV}^{*}>$	0.9983	0.9946	0.9986	$<S_{VV}S_{VV}^{*}>$	0.9980	0.9915	0.9952
$<S_{HV}S_{HV}^{*}>$	0.9989	0.9967	0.9974	$<S_{HV}S_{HV}^{*}>$	0.9971	0.9877	0.9902
$Re<S_{HH}S_{VV}^{*}>$	0.9975	0.9935	0.9975	$Re<S_{HH}S_{VV}^{*}>$	0.9960	0.9238	0.9753
$Im<S_{HH}S_{VV}^{*}>$	0.9991	0.9962	0.9938	$Im<S_{HH}S_{VV}^{*}>$	0.9996	0.9788	0.9287

Table 3. Error Matrix for the Results of Maximum Likelihood Classification of the AirSAR Data. The Field Data is Shown in the Columns of the Table.

	1	2	3	4	5	6	PA
1:*Eucalypt* open forest	91.6	4.8	0.0	0.0	0.0	3.6	91.6
2:*Eucalypt* woodland	7.1	83.3	0.0	0.0	7.1	2.4	83.3
3:Closed Forest	3.2	0.0	90.3	3.2	3.2	0.0	90.3
4:Pine	0.0	0.0	3.3	96.7	0.0	0.0	96.7
5:Mangroves	0.0	10.3	3.4	0.0	86.2	0.0	86.2
6:*Melaleuca* open forest	11.4	11.4	5.7	0.0	0.0	71.4	71.4
				Overall accuracy:			**87.2**
				Kappa coefficient:			**0.84**

Figure 5 contains four graphs for the respective channels in C-Band. The incidence angle is graphed on the x-axis in degrees. The y-axis cover the range of data values (Intensity for magnitude of HH, VV, and HV backscatter) present in the channel for raw data, the LUT correction and the Slope correction method. The data values are the average of data values observed at each incidence angle within pixels designated as Eucalypt Woodland communities by a Landsat TM classification of the study area. The angular dependence of the raw data can be clearly seen. The HH polarization data is well represented as a linear relationship. The VV, HV and real part of the co-polarized return data exhibit an inverse relationship with incidence angle below 40 degrees. In the range of 40 to 60 degrees there is little change with angular variation, followed by a rapid decrease in the very far range. The imaginary part of the co-polarized return is positively related to the incidence angle and also shows little variation above a 40 degree incidence angle. The resulting image data after the correction procedure has been applied is shown in figure 6. The brightness variation with incidence angle observed in the raw data (figure 2) has clearly been diminished.

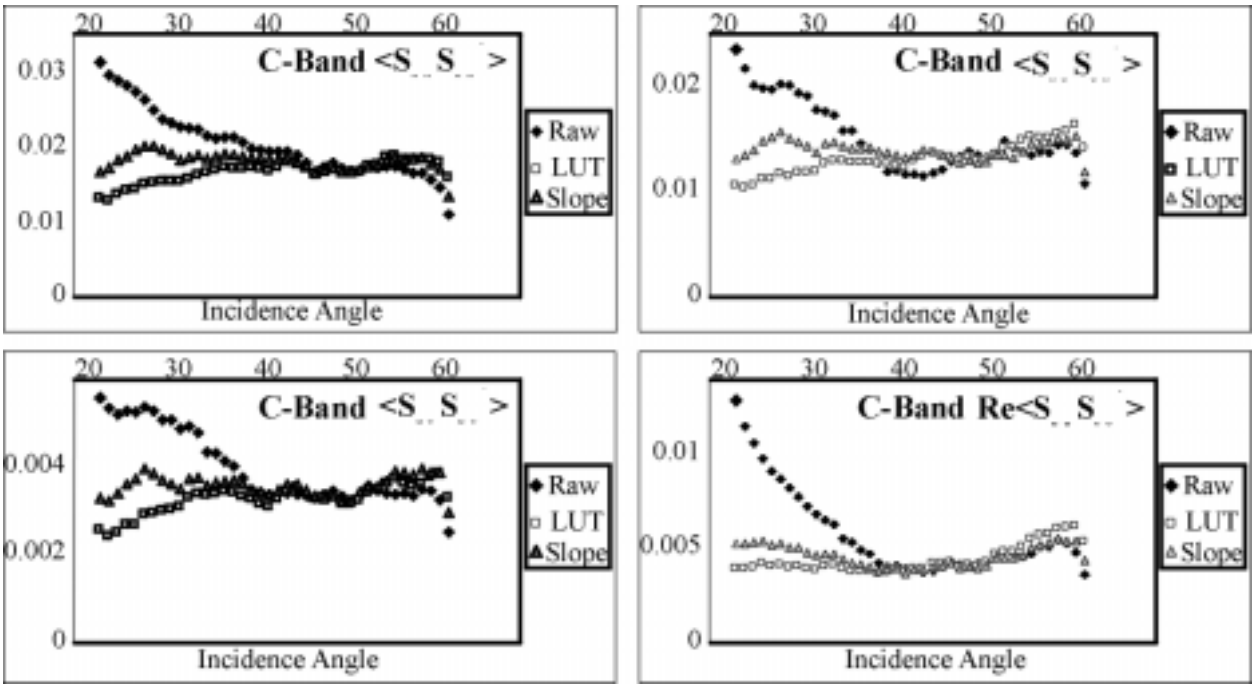

Figure 5. *Average SAR values for the cover type Eucalypt Woodland are graphed versus incidence angle for raw and corrected AirSAR data.*

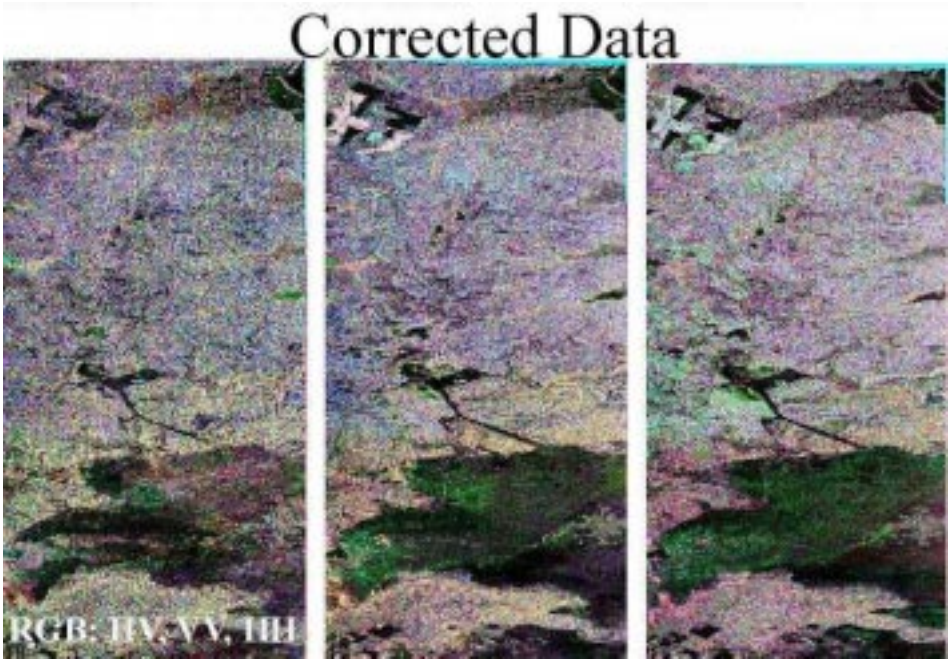

Figure 6. *Colour composites of the incidence angle corrected AirSAR data showing the HV, VV, and HH polarizations as RGB for the C-,L- and P-Band.*

Figure 7 is the result of a Maximum Likelihood classification performed on the incidence angle corrected data. The associated error matrix derived from a total of 250 ground truth data points is shown in table 3. The accuracy of the classification achieved 87.2% for the discrimination of Mangroves, *Melaleuca* Forest, Pine Forest, *Eucalypt* forest, *Eucalypt* Woodland and Closed Forest communities. The lowest class accuracy was obtained for the *Melaleuca* communities, with 71%. Considerable overlap occurred with the Eucalypt woodland and open forest communities. The ground truth data was collected by noting the tree density as well as the dominant species. Whether a Eucalypt community was dominated by Eucalyptus *miniata*, *tetrodonta* or *bleeseri* was, however, not reflected in the analysis of the AirSAR data using the methodology described. As structural differences between these tree species is minimal, this result was to be expected. The ability to differentiate the species *Melaleuca*, even at a lower success rate, is most likely due to this species inhabiting swamps and floodplains and often growing in uniform stands.

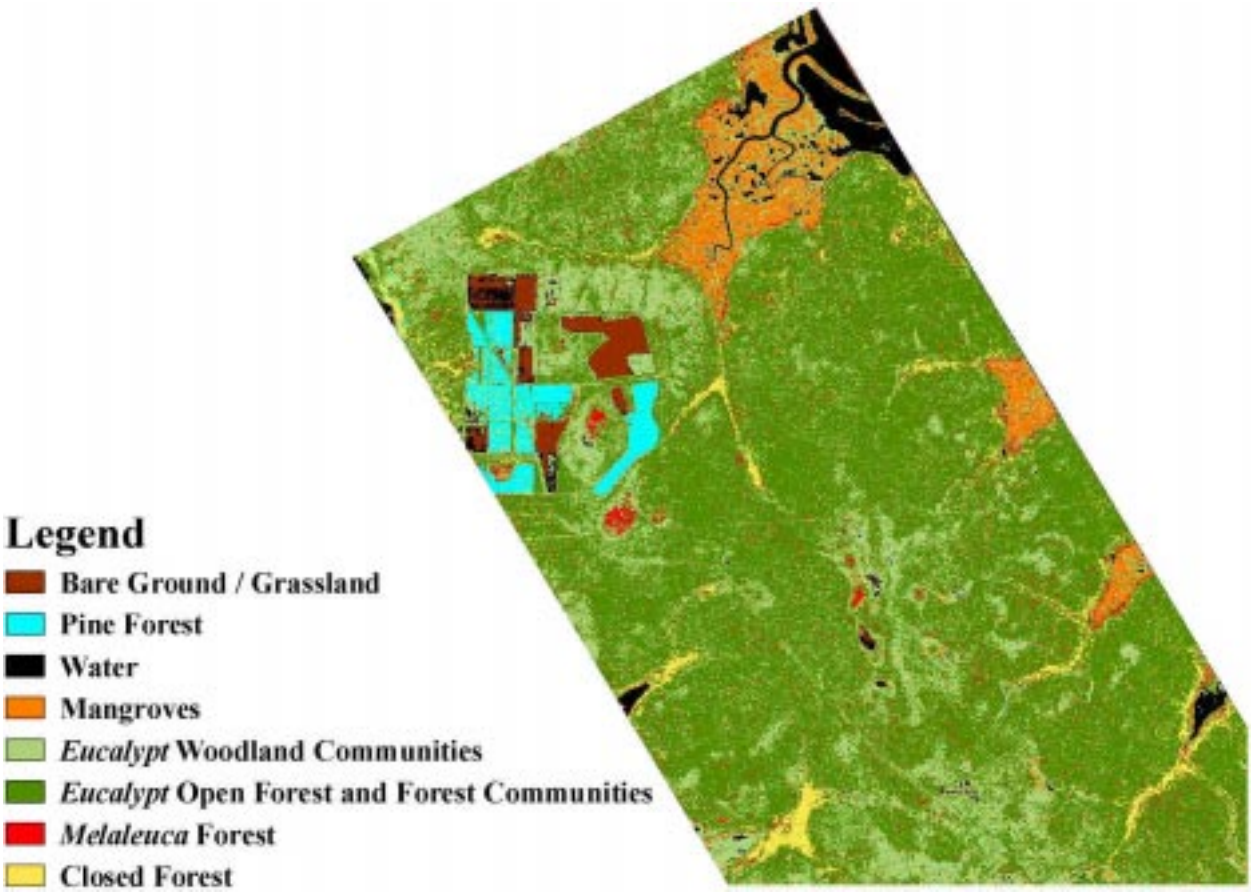

Figure 7. *Classified AirSAR data for the northern part of the study area.*

The class of *Eucalypt* open forest/ forest encompasses the largest percentage of the study area. An unsupervised classification implemented on only those image elements belonging to this class resulted in spatially contiguous classes as shown in figure 8. The available ground truth did not allow interpretation of these classes. Further research is required to identify the biophysical variable(s) responsible for this differentiation.

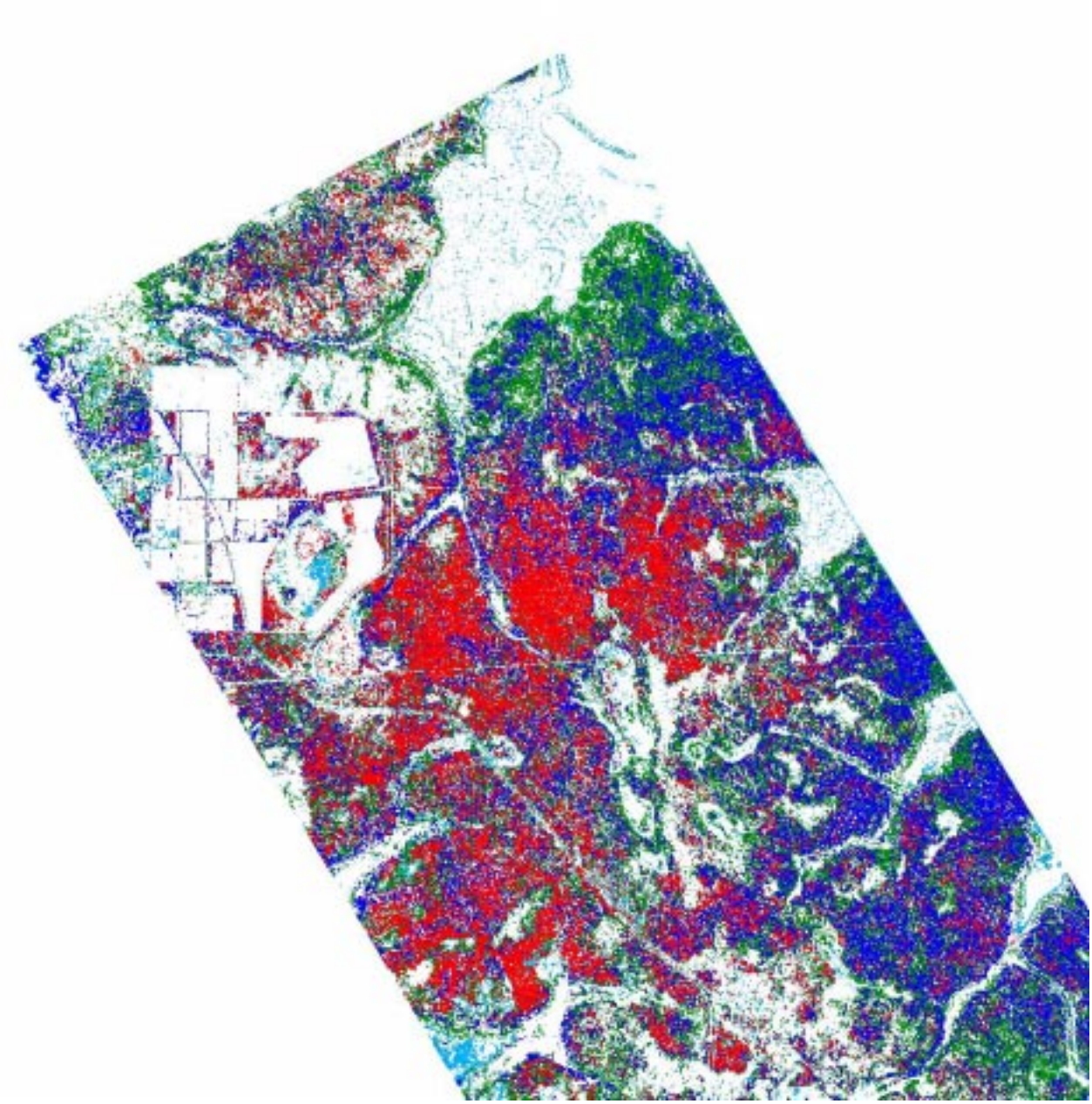

Figure 8. *Results of a further segmentation of the data resulting in distinct classes that are not supported by currently available ground truth.*

5. CONCLUSION

The advance of radar remote sensing in the general remote sensing community is hindered by the need for highly specialized analysis methods. The mathematical modeling of microwave interactions with ground cover was instrumental in illuminating the properties of radar imagery, but are too complex to allow image interpretation, especially in natural

environments. The side looking nature of active radar sensors introduces geometric distortions and effects due to variation in incidence angle that make radar imagery unsuitable to standard processing techniques. This paper has shown that the incidence angle effects can be removed from radar data, rendering it in a format that allows comparative discrimination of land cover types using standard image processing algorithms implemented in commercially available software. The accuracy of the classification achieved 87.2% for the discrimination of Mangroves, *Melaleuca* Forest, Pine Forest, *Eucalypt* forest, *Eucalypt* Woodland and Closed Forest communities. The discrimination of two open forest communities dominated by different species was unsatisfactory. It is possible to conjecture that structural differences between vegetation communities must exist for radar imagery to allow discrimination.

6. ACKNOWLEDGMENTS

The authors would like to acknowledge the financial assistance of the Cooperative Research Centre for the Sustainable Development of Tropical Savannas.

7. REFERENCES

Ahmad, W., O'Grady, A. P., Pfitzner, K., and Hill, G. J. E., (1997), Use of multispectral scanner data for the identification and mapping of tropical forests of northern Australia, in *Forests at the Limit: Environmental Constraints on Forest Function. International Union of Forest Research Organistaions Workshop*, Skukuza, Kruger National Park, South Africa.

Baker, J. R., Mitchell, P. L., Cordey, R. A., Groom, G. B., Settle, J. J., and Stileman, M. R., (1994), Relationship Between Physical Characteristics and Polarimetric Radar Backscatter for Corsican Pine Stands in Thetford Forest, U.K., *International Journal of Remote Sensing*, 15: 2827-2849.

Borgeaud, M., (1994), Analysis of Theoretical Surface Scattering Models for Polarimetric Microwave Remote Sensing of Bare Soils, *International Journal of Remote Sensing*, 15: 2931-2942.

Chauhan, N. S., Lang, R. H., and Ranson, K. J., (1991), Radar Modeling of a Boreal Forest, *IEEE Transactions on Geoscience and Remote Sensing*, 29: 627-638.

Cloude, S.R., (1992), Uniqueness of Target Decomposition Theorems in Radar Polarimetry. *Direct and Inverse Methods in Radar Polarimetry*, Part 1, Boerner, W-M. et al., eds. Kluwer Academic Publishers, New York:267-296.

Cloude, S.R. and Pottier, E.,(1996), A review of Target Decomposition Theorems in Radar Polarimetry, *IEEE Transactions on Geoscience and Remote Sensing*, 34: 498-518.

Cloude, S.R. and K. P. Papathanassiou, (1997). Polarimetric Optimization in Radar/SAR interferometry, *Electronic Letters*,33, 18.

De Grandi, G. F., Lemoine, G. G., De Groof, H., Lavalle, C., and Sieber, A. J., (1994), Fully Polarimetric Classification of the Black Forest MAESTRO 1 AIRSAR Data, *International Journal of Remote Sensing*, 15: 2755-2775.

Dobson, M. C., Ulaby, F. T., LeToan, T., Beaudoin, A., Kasischke, E. S., and Christensen, N., (1992), Dependence of Radar Backscatter on Coniferous Forest Biomass., *IEEE Transactions on Geoscience and Remote Sensing*, 30: 412-416.

Dong, Y., Richards, A., and Cashman, J., (1995), A Model of Volume Attenuation and Backscattering by Foliage at L- and P- Bands, *International Journal of Remote Sensing*, 16: 1231-1247.

Dong, Y., Forster, B., and Milne, A., (1998), Segmentation and Classification of Single / Multi - Channel Radar Imagery Using Gaussian Markov Random Model, in *9th Australasian Remote sensing and Photogrammetry Conference*, Sydney, Australia, (Sydney: Causal Productions), 20-24th July ,CDRom, #96.

Du, L. and Lee, J. S., (1996), Fuzzy Classification of Earth Terrain Covers using Complex Polarimetric SAR Data, *International Journal of Remote Sensing*, 17: 809-826.

Durden, S. L., van Zyl, J. J., and Zebker, H. A., (1989), Modeling and Observation of the Radar Polarization Signature of Forested Areas, *IEEE Transactions on Geoscience and Remote Sensing*, 27: 290-299.

Foody, G. M., Green, R. M., Lucas, R. M., Curran, P. J., Honzak, M., and Amaral, I. D., (1997), Observations on the Relationship Between SIR-C Radar Backscatter and the Biomass of Regenerating tropical forests, *International Journal of Remote Sensing*, 18: 687-694.

Harrell, P. A., Kasischke, E. S., Bourgeau_Chavez, L. L., Haney, E. M., and Christensen Jr., N. L., (1997), Evaluation of Approaches to Estimating Aboveground Biomass in Southern Pine Forests Using SIR-C Data, *Remote Sensing of Environment*, 59: 223-233.

Hess, L. L., Melack, J. M., Filoso, S., and Wang, Y., (1995), Delineation of Inundated Area and Vegetation along the Amazon Floodplain with the SIR-C synthetic Aperture Radar, *IEEE Transactions on Geoscience and Remote Sensing*, 33: 896-904.

Hickey, S. H., (1985), *Northern Territory Geological Survey*, Department of Mines and Energy, Darwin, Australia.

Hussin, Y. A., Reich, R. M., and Hoffer, R. M., (1991), Estimating Slash Pine Biomass Using Radar Backscatter, *IEEE Transactions on Geoscience and Remote Sensing*, 29: 427-431.

Imhoff, M. L., Sisk, T. D., Milne, A., Morgan, G., and Orr, T., (1997), Remotely Sensed Indicators of Habitat Heterogeneity: Use of Synthetic Aperture Radar in Mapping Vegetation Structure and Bird Habitat, *Remote Sensing of Environment*, 60: 217-227.

Lemoine, G., Grandi, G. F., and Sieber, A. J., (1994), Polarimetric Contrast Classification of Agricultural Fields using MAESTRO 1 AIRSAR Data, *International Journal of Remote Sensing*, 15: 2851-2869.

Kasischke, E. S., Bourgeau, L. L., Christensen, J. N. L., and Haney, E., (1994), Observations on the Sensitivity of ERS-1 SAR Image Intensity to Changes in Aboveground Biomass in Young Loblolly Pine Forests, *International Journal of Remote Sensing*, 15: 3-16.

Kasischke, E. S., Melack, J. M., and Dobson, M. C., (1997), The Use of Imaging Radars for Ecological Applications - A Review, *Remote Sensing of Environment*, 59: 141-156.

McDonald, K. C. and Ulaby, F. T., (1993), Radiative Transfer Modelling of Discontinuous Tree Canopies at Microwave Frequencies, *International Journal of Remote Sensing*, 14: 2097-2128.

Menges, C., Crerar, J., Ahmad, W., and Hill, G. J. E., (1998), A Method for Estimating the Effect of Variation in Local Incidence Angle on AirSAR Data, in *9th Australasian Remote sensing and Photogrammetry Conference*, Sydney, Australia, (Sydney: Causal Productions), 20-24th July ,CDRom, #145.

Menges, C., van Zyl, J. J., Hill, G. J. E., and Ahmad, W., (1999a), A Procedure for the Correction of the Effect of Variation in Local Incidence Angle on AIRSAR Data, *International Journal of Remote Sensing*: (submitted).

Menges, C., Hill, G. J. E., Ahmad, W., and van Zyl, J. J., (1999b), An Evaluation of Three Alternative Procedures for the Correction of the Effect of Variation in Local Incidence Angle on AirSAR Data, *Photogrammetric Engineering & Remote Sensing*: (submitted).

Menges, C., Hill, G. J. E., and Ahmad, W., (1999c), Use of Airborne Video Data for the Characterisation of Tropical Savannas in Northern Australia: The Optimal Spatial Resolution for Remote Sensing Applications, *International Journal of Remote Sensing*: (submitted).

Menges, C., Hill, G. J. E., and Ahmad, W., (1999d), Evaluation of AIRSAR data for the classification of vegetation communities in the tropical savannas of northern Australia, *4th North Australian Remote Sensing and GIS conference*, Darwin, Australia, 28-30th June, (in press).

Ranson, K. J. and Sun, G., (1994), Northern Forest Classification Using Temporal Multifrequency and Multipolarimetric SAR Images, *Remote Sensing of Environment*, 47: 142-153.

Ranson, K. J. and Sun, G., (1997), An Evaluation of AIRSAR and SIR-C/X-SAR Images for Mapping Northern Forest Attributes in Maine, USA, *Remote Sensing of Environment*, 59: 203-222.

Rauste, Y., Haeme, T., Pulliainen, J., Heiska, K., and Hallikainen, M., (1994), Radar-Based Forest Biomass Estimation, *International Journal of Remote Sensing*, 15: 2797-2808.

Rignot, E. and Chellappa, R., (1992), Segmentation of Polarimetric Synthetic Aperture Radar Data, *IEEE Transactions on Image Processing*, 1: 281-299.

Rignot, E., Way, J., Williams, C., and Viereck, L., (1994a), Radar Estimates of Aboveground Biomass in Boreal Forests of Interior Alaska, *IEEE Transactions on Geoscience and Remote Sensing*, 32: 1117-1124.

Rignot, E. J. M., Williams, C. L., Way, J., and Viereck, L. A., (1994b), Mapping of Forest Types in Alaskan Boreal Forests Using SAR Imagery, *IEEE Transactions on Geoscience and Remote Sensing*, 32: 1051-1059.

Rignot, E., Salas, W. A., and Skole, D. L., (1997), Mapping Deforestation and Secondary Growth in Rondonia, Brazil, Using Imaging Radar and Thematic Mapper Data, *Remote Sensing of Environment*, 59: 167-179.

Rosenqvist, A., (1996), Evaluation of JERS-1, ERS-1 and Almaz SAR Backscatter for Rubber and Oil Palm Stands in West Malaysia, *International Journal of Remote Sensing*, 17: 3219-3231.

Saatchi, S. S., Soares, J. V., and Alves, D. S., (1997), Mapping Deforestation and Land Use in Amazon Rainforest by Using SIR-C Imagery, *Remote Sensing of Environment*, 59: 191-202.

Sun, G., Simonett, D. S., and Strahler, A. H., (1991), A Radar Backscatter Model for Discontinuous Coniferous Forests, *IEEE Transactions on Geoscience and Remote Sensing*, 29: 639-644.

Sun, G., Simonett, D. S., and Strahler, A. H., (1991), A Radar Backscatter Model for Discontinuous Coniferous Forests, *IEEE Transactions on Geoscience and Remote Sensing*, 29: 639-644.

Van Zyl, J. J. and Ulaby, F. T., (1990), Scattering matrix representation for simple targets, in *Radar Polarimetry for Geoscience Applications*, Ulaby and Elachi: Artech House, Inc., Ch 2.

Wang, Y., Day, J., and Sun, G., (1993a), Santa Barbara Microwave Backscattering Model for Woodlands, *International Journal of Remote Sensing*, 14: 1477-1493.

Wang, Y., Davis, F. W., and Melack, J. M., (1993b), Simulated and Observed Backscatter at P-, L-, and C-Bands from Ponderosa Pine Stands, *IEEE Transactions on Geoscience and Remote Sensing*, 31: 871-879.

Wang, Y., Day, J. L., Davis, F. W., and Melack, J. M., (1993c), Modeling L-Band Radar Backscatter of Alaskan Boreal Forest, *IEEE Transactions on Geoscience and Remote Sensing*, 31: 1146-1154.

Wang, Y., Davis, F. W., Melack, J. M., Kasischke, E. S.,, and Christensen, J. N. L., (1995), The Effects of Changes in Forest Biomass on Radar Backscatter form Tree CanopiesInternational Journal of Remote Sensing, *International Journal of Remote Sensing*, 16: 503-513.

Wilson, B.A; Brocklehurst, P.S; Clark, M.J and Dickinson, K.J.M (1990). Vegetation survey of the Northern Territory, Australia. Conservation Commission of the Northern Territory, Technical Report No 49.

Yanasse, C. C. F., Sant'Anna, S. J. S., Frery, A. C., Renno, C. D., Soares, J. V., and Luckman, A. J., (1997), Exploratory Study of the Relationship Between Tropical Forest Regeneration Stages and SIR-C L and C Data, *Remote Sensing of Environment*, 59: 180-190.

Zebker , H. A. and van Zyl, J. J., (1991), Imaging Polarimetry: A Review, *Proceedings of the IEEE*, 79: 1583-1606.